2000

REPORT DOCUMENTATION PAGE

AFRL-SR-BL-TR-00-

0557

1. REPORT DATE (DD-MM-YYYY)	2. REPORT TYPE	3. DATES COVERED (From - To)
2000	Final Technical Report	15/07/1996 – 30/09/1999

4. TITLE AND SUBTITLE

An Analytical and Numerical Investigation of Failure Waves

5a. CONTRACT NUMBER

5b. GRANT NUMBER
F49620-96-1-0381

5c. PROGRAM ELEMENT NUMBER

6. AUTHOR(S)

Zhen Chen

5d. PROJECT NUMBER

5e. TASK NUMBER

5f. WORK UNIT NUMBER

7. PERFORMING ORGANIZATION NAME(S) AND ADDRESS(ES)

The Curators of the University of Missouri
for the University of Missouri-Columbia
310 Jesse Hall
Columbia MO 65211

CAGE Code 4B849
CFDA #12.800

8. PERFORMING ORGANIZATION REPORT NUMBER
C-5-34005

9. SPONSORING/MONITORING AGENCY NAME(S) AND ADDRESS(ES)

AFOSR/PKA
801 N Randolph St Room 732
Arlington VA 22203-1977

10. SPONSOR/MONITOR'S ACRONYM(S)
AFOSR/PKA

11. SPONSOR/MONITOR'S REPORT NUMBER(S)

12. DISTRIBUTION/AVAILABILITY STATEMENT

Unclassified Unlimited Distribution

20001024 120

13. SUPPLEMENTARY NOTES

14. ABSTRACT

~~Based on the proposed research plan, an analytical and numerical investigation has been~~ performed on the failure wave phenomenon. It appears that progressive percolation of microfissures into the material bulk governs the failure wave mechanisms. A three-dimensional damage diffusion model has been developed based on the assumption of shear-induced dilatancy. Because of the termination of the Shock Physics Program, no consistent experimental data could be obtained from other researchers supported under this program to explore the failure waves in geologic materials. Hence, the shock experiments on glass specimens have been considered to verify the proposed modeling and simulation approaches. The constitutive model has been implemented into the computer programs by using both the finite element and material point methods. The numerical solutions obtained by different methods are consistent, and the comparisons with experimental data are reasonable.

15. SUBJECT TERMS

Failure Wave, Damage Diffusion, Shear-Induced Dilatancy,
Jump Conditions, Material Point Method, The Transition among PDE

16. SECURITY CLASSIFICATION OF:			17. LIMITATION OF ABSTRACT	18. NUMBER OF PAGES	19a. NAME OF RESPONSIBLE PERSON
a. REPORT	b. ABSTRACT	c. THIS PAGE			Zhen Chen
N/A	N/A	N/A	UU	25	19b. TELEPHONE NUMBER (Include area code) (573) 882-0311

AN ANALYTICAL AND NUMERICAL INVESTIGATION ON FAILURE WAVES

Abstract

When a glass specimen is shocked near but below the apparent Hugoniot elastic limit, it may undergo elastic deformations at the shock wave front, and fail catastrophically at a later time. Because such a phenomenon looks different from usual inelastic waves, it has been interpreted as a failure wave. Based on the observation that the failure wave propagates with a degraded speed at some distance behind the elastic shock wave front, it has been proposed that the progressive percolation of microfissures into the material bulk governs the failure wave mechanisms. Stress concentration due to the defects and transient loading conditions on the impact surface has been assumed to be the origin for initiating the evolution of heterogeneous microdamage. To provide a general framework for modeling the impact response of certain materials, a three-dimensional continuum damage model is developed in this report, based on the assumption of shear-induced dilatancy. The essential component of the proposed model is that the deviatoric potential energy in the intact material is converted into the volumetric potential energy in the comminuted and dilated material during the time-dependent failure evolution process. The progressive percolation of microfissures is described by a nonlinear diffusion equation throughout the continuum body. The diffusion equation and wave equation are then solved via a staggered manner in a single computational domain. Numerical solutions are presented and verified with experimental data available. It appears that the essential feature of the failure wave phenomenon, as observed in shock experiments on glasses, can be predicted by the proposed approach. A very recent experimental study indicates that the dynamic failure evolution in mortar is a rather gradual process, in contrast to the well-defined failure wave front as observed in shocked glasses. However, the lack of a consistent set of experimental data does not warrant the revision of the proposed constitutive model to predict the failure wave in mortar. Although a considerable progress has been made in understanding the failure wave phenomenon since it was reported about 10 years ago, a combined experimental, analytical and computational effort is still needed to fully understand the physics involved in the dynamic failure behaviors of brittle solids under various impact loads.

1. Introduction

When a glass specimen is shocked near but below the apparent Hugoniot elastic limit (HEL), it may undergo elastic deformations at the shock wave front, and fail catastrophically at a later time. Because such a phenomenon looks different from usual inelastic waves, it has been interpreted as a failure wave. Since Brar et al. (1991) and Kanel et al. (1991) reported the formation and propagation of failure waves in a series of impact experiments with glass plates and bars, continued efforts have been made to explore this interesting physical phenomenon (Bless and Brar, 1994; Bourne et al., 1995; Chen and Xin, 1999; Clifton, 1993; Espinosa et al., 1997a and b; Feng, 2000; Grady, 1995a and b; Grote et al., 2000; Raiser and Clifton, 1994; Raiser et al., 1994; Rosenberg et al., 1996; among others). However, no consensus can be made at the moment on the physics behind the failure wave phenomenon in brittle solids under impact loading. To set a stage for presenting the proposed damage model, the difference between a usual inelastic wave and the failure wave is first analyzed, based on the literature available, as below.

The shock response of glasses beyond the HEL often displays a well-defined two-wave structure that has been interpreted as an inelastic response. Although the prompt microcracking across the compression wave front occurs if the glass specimen is shocked at or above the HEL, the macroscopic two-wave structure has suggested that the compressive failure might be suppressed by confining pressure at a shocked state beyond the HEL. The failure wave phenomenon of glasses, which occurs when the compressive shock stress is near but below the HEL, suggests that the HEL may not be an elastic limit, but rather, may be a transition in failure mechanisms. A possible transition is the one from a delayed kinetic-controlled failure process below the HEL to a prompt stress-controlled failure process above the HEL (Grady, 1995b). Another possibility is that the HEL may represent the stress level above which bulk glass undergoes permanent densification (Espinosa et al., 1997a). In other words, the density of glass rubble due to the failure below the HEL is different from that above the HEL. The signature feature that separates the failure wave from the usual inelastic shock wave in brittle solids is that only the lateral stress is changed significantly across the failure front, while the

longitudinal stress is almost constant during the failure propagation (Brar et al., 1991; Kanel et al., 1991; Bourne et al., 1995; Espinosa et al., 1997a). Thus, the classical equation of motion governing the propagation of a longitudinal wave can not describe the propagation of a failure wave with the decrease in shear strength only, if other field equations are not invoked.

Based on a detailed review of experimental, analytical and computational issues related to the failure wave phenomenon, attempts (Chen and Xin, 1999; Feng, 2000) have been made recently to answer the fundamental question: what is the physical mechanism behind the failure wave phenomenon?

As indicated in the previous research, the jumps of certain kinematic field variables involved in a complete failure process can be identified based on the transition between different governing differential equations (Chen, 1996; Chen and Sulsky, 1995). By taking the initial point of material failure as that point where the type of the governing differential equations changes, i.e., a hyperbolic to an elliptic type for dynamic problems and an elliptic to another elliptic type for static problems, a moving material surface of discontinuity can be defined through the jump forms of conservation laws across the surface. Jumps in density, velocity, strain and stress can be accommodated on this moving surface of discontinuity between two material domains. Interestingly, the problems involving the type change of the governing differential equations, accompanied by certain jumps in field variables, also occur in other areas such as fluid mechanics (Chen and Clark, 1995) and thermal shock wave propagation (Tzou, 1989 and 1997).

Mathematically speaking, three basic kinds of governing differential equations, namely, hyperbolic (wave), parabolic (diffusion) and elliptic (instantaneous response through the problem domain) equations, have been used to describe different physical phenomena. However, it is still an unsolved challenging problem how to represent the transition among these three different kinds of equations within a rigorous mathematical framework. If the transition from a hyperbolic one to an elliptic one is represented via a parabolic one, an analytical solution has been obtained for a dynamic softening bar with the use of a simple elastoplasticity model (Xin and Chen, 2000). The use of the jump forms of conservation laws, together with a simple elastodamage model, also yields a diffusing failure front (Chen and Xin, 1999). If the failure wave were really a "wave," its propagation speed should increase during the failure process because the material

stiffness behind the failure front is weaker than that in front of it due to the evolution of microcracking in space. As observed in experiments, however, the time delay between the elastic shock wave front and the eruption of failure appears to increase with the distance into the material. From both experimental and analytical viewpoints, therefore, it appears that the evolution of a failure wave in space should be governed by a diffusion equation instead of a wave equation. Since it is still impossible to measure the real-time internal failure evolution, it is difficult to fully understand the physical mechanism behind the failure wave phenomenon. Based on the experimental data available, nevertheless, a micromechanics-based picture has been drawn to explain the physical mechanism of failure waves (Feng, 2000), as sketched as follows.

Under plane shock wave loading, the material failure below the HEL occurs through simultaneous processes of heterogeneous microfissuring, shear dilatancy and void collapsing under very high confining stress, which results in an increase in the mean stress and a decrease in the deviatoric stress while all the longitudinal field variables remain unchanged. This particular form of failure initiates at the impact surface where the surface defects and transient loading conditions are conducive for such a process, and propagates into the material bulk through progressive multiplication of microfissures – a percolation process. As a result, the failure propagation is of diffusive nature. In analogy to the definition of permanent inelastic strain, the dilated volume of the damaged material at full release can be employed to measure the extent of microdamage, rendering an internal state variable approach for the constitutive modeling of failure waves.

A recent experimental study on the failure response of mortar under impact loading indicates that a clearly defined failure front can not be observed, and instead, a gradual failure process occurs upon the arrival of the loading wave and propagates thereafter (Grote et al., 2000). The difference in the speed of failure eruption between glass and mortar materials seems to be related to the fact that virgin mortar is heterogeneous with many voids as compared with virgin glass. There would not be such a difference if the failure propagation is not of diffusive nature. To better understand the difference between different materials, however, well-designed experiments are still required to obtain a consistent set of experimental data.

To provide a general framework for modeling the impact response of certain brittle solids, a three-dimensional continuum damage model is developed here, based on

the assumption of shear-induced dilatancy. The essential component of the proposed model is that the deviatoric potential energy in the intact material is converted into the volumetric potential energy in the comminuted and dilated material during the time-dependent failure evolution process. The progressive percolation of microfissures is described by a nonlinear diffusion equation throughout the continuum body. The diffusion equation and wave equation are then solved via a staggered manner in a single computational domain. Numerical solutions are presented and verified with experimental data available to demonstrate the applicability of the proposed procedure. Future research is discussed based on the conclusion of the current work.

2. Constitutive Modeling

A direct notation is employed here with boldfaced letters denoting tensors of first or higher order. The Cauchy stress and velocity strain tensors are used to implement the proposed continuum damage model into the finite element program with an updated Lagrangian formulation, as discussed later in the next section. The thermal effects are not considered here for the purpose of simplicity.

In the shocked intact material, the compressive mean stress can be expressed as

$$\sigma_m = H(\mu) \tag{1a}$$

with

$$\mu = \frac{V_0}{V} - 1 \tag{1b}$$

where H is the Hugoniot mean stress response of the material, depending on the volume compression, μ, in the elastically shocked state where the dilated volume V_d of the damaged material is equal to zero In Eq. (1b), V and V_0 denote the current and original specific volume, respectively. Once the failure wave is initiated, σ_m and V_d start to increase with damage at a fixed value of μ. In other words, there is no macroscopic volume change during the failure evolution, and the uniaxial-strain condition is preserved at the macroscopic level for the plate impact problem. This failure response is modeled by assuming that

$$\sigma_m = H(\mu_e) \tag{2a}$$

with

$$\mu_e = \mu + \frac{V_d}{V} = \frac{V_0 + V_d}{V} - 1 = \frac{\rho}{\rho_0} + \rho V_d - 1 \tag{2b}$$

in which ρ and ρ_0 represent the current and original mass density, respectively. Although Eq. (2) represents a phenomenological approximation, it is expected to be useful as long as the damaged material is sufficiently compressed. In fact, μ_e can be considered as the average solid volume compression of the damaged material. Based on the experimental data available, the Hugoniot mean stress response can then be described by a polynomial function of μ_e, namely

$$\sigma_m = a_1\mu_e + a_2\mu_e^2 + a_3\mu_e^3 \tag{3}$$

while the pressure-dependent shear modulus can be defined in terms of a polynomial of σ_m, i.e.,

$$G = b_0 + b_1\sigma_m + b_2\sigma_m^2 + b_3\sigma_m^3 \tag{4}$$

in which a_i and b_i are model parameters to be determined from shock experiments. The differential form of Eq. (3) can be written as

$$d\sigma_m = \frac{\partial \sigma_m}{\partial V} dV + \frac{\partial \sigma_m}{\partial V_d} dV_d \tag{5a}$$

with

$$\frac{\partial \sigma_m}{\partial V} = -\left(a_1 + 2a_2\mu_e + 3a_3\mu_e^2\right)\frac{V_0 + V_d}{V^2} \tag{5b}$$

$$\frac{\partial \sigma_m}{\partial V_d} = \left(a_1 + 2a_2\mu_e + 3a_3\mu_e^2\right)\frac{1}{V} \tag{5c}$$

With $\boldsymbol{s}_d = \boldsymbol{s} - \boldsymbol{s}_v$ and $\boldsymbol{e}_d = \boldsymbol{e} - \boldsymbol{e}_v$ denoting deviatoric stress and strain tensors, respectively, the differential deviatoric stress-strain relationship takes the form of

$$d\boldsymbol{s}_d = 2G\left(d\boldsymbol{e}_d - d\boldsymbol{e}_d^i\right) \tag{6}$$

in which $\boldsymbol{e}_d^i$ is the inelastic deviatoric strain due to shear-induced dilatancy. With $\boldsymbol{i}$ being the second order identity tensor, $\boldsymbol{s}_v = -\sigma_m\boldsymbol{i}$ and $\boldsymbol{e}_v = \varepsilon_m\boldsymbol{i}$ represent the volumetric parts of stress and strain, respectively. The mean volumetric strain, ε_m, is defined to be

$$3\varepsilon_m = ln\frac{V}{V_0} = 3\varepsilon_m^e + 3\varepsilon_m^i \tag{7}$$

Imagining that the material is compressed from an initial porous state ($V_0 + V_d$) to the current state (V), the inelastic mean volumetric strain can be represented by

$$3\varepsilon_m^i = ln\frac{V_0 + V_d}{V_0} \tag{8}$$

It then follows from Eqs. (7) and (8) that the elastic mean volumetric strain can be found to be $3\varepsilon_m^e = ln\frac{V}{V_0 + V_d}$. Please note that there is no permanent volume compression in the kinematics of failure wave considered here. Damage evolution does not change the current volume, and instead, changes the material state at full unloading. In other words, the condition of $V_d = 0$ results in a null ε_m^i. To calculate $\boldsymbol{e}_d^i$, assume that there exists a limit surface given by

$$f = W_v^e + W_d^e - c = 0 \tag{9}$$

where W_v^e and W_d^e are the volumetric and deviatoric parts of elastic potential energy, respectively, and c represents the limit state at which failure occurs. The corresponding consistency condition can be written as

$$df = dW_v^e + dW_d^e = 0 \tag{10a}$$

namely

$$\boldsymbol{s}_v : d\boldsymbol{e}_v^e + \boldsymbol{s}_d : d\boldsymbol{e}_d^e = 0 \tag{10b}$$

The kinematics of failure wave under plate impact implies the condition of $d\boldsymbol{e}_v = d\boldsymbol{e}_d = \boldsymbol{0}$. In other words, the failure wave behind the shock wave front will not introduce any additional strain at the macroscopic level, as discussed before. As a result, the relationships between the elastic and inelastic parts of volumetric and deviatoric strains have the form of

$$d\boldsymbol{e}_v^e = -d\boldsymbol{e}_v^i = -\frac{dV_d}{3(V_0 + V_d)}\boldsymbol{i} \tag{11a}$$

and

$$d\boldsymbol{e}_d^e = -d\boldsymbol{e}_d^i \tag{11b}$$

respectively. With the use of Eqs. (10) and (11), hence, it follows that

$$\frac{\sigma_m}{V_0 + V_d} dV_d - \boldsymbol{s}_d : d\boldsymbol{e}_d^i = 0 \tag{12}$$

With the assumption of

$$de_d^i = d\lambda s_d \tag{13}$$

the substitution of Eq. (13) into Eq. (12) then yields

$$d\lambda = \frac{\sigma_m}{(V_0 + V_d)s_d : s_d} dV_d > 0 \tag{14}$$

because of $dV_d > 0$ with the evolution of failure. Thus, the differential inelastic deviatoric strain tensor takes the form of

$$de_d^i = \frac{\sigma_m s_d}{(V_0 + V_d)s_d : s_d} dV_d \tag{15}$$

The three-dimensional isotropic damage model with shear-induced dilatancy is now complete for the given strain state in shocked materials under plate impact. As can be seen from the above equations, the stress state depends on the value of V_d for the given strain state after material failure occurs behind the elastic shock wave.

For each time increment Δt, the solution steps of a simple constitutive model solver can be summarized as follows:

1. $\mu_e = \frac{V_0 + V_d|^t}{V|^t} - 1$ with $V_d|^t = V_d|^{t-\Delta t} + \Delta V_d$;
2. $\sigma_m = a_1\mu_e + a_2\mu_e^2 + a_3\mu_e^3$;
3. $G = b_0 + b_1\sigma_m + b_2\sigma_m^2 + b_3\sigma_m^3$;
4. $\Delta e_d^i = \frac{\sigma_m s_d}{(V_0 + V_d|^t)s_d : s_d} \Delta V_d$;
5. $\Delta s_d = 2G(\Delta e_d - \Delta e_d^i)$ with $\Delta e_d = \Delta e - \Delta e_v$ and $\Delta e_v = e_v|^t - e_v|^{t-\Delta t}$; and
6. $s|^t = s|^{t-\Delta t} + \Delta s$ with $\Delta s = \Delta s_d + (-\Delta\sigma_m)i$ and $\Delta\sigma_m = \sigma_m|^t - \sigma_m|^{t-\Delta t}$.

Please notice that $\Delta e \neq 0$ and $\Delta V_d = 0$ in the elastic shock wave zone, while $\Delta e = 0$ and $\Delta V_d > 0$ behind the elastic shock wave if failure occurs. The value of V_d is obtained from the damage diffusion equation, as described later.

To demonstrate the features of the proposed damage model, consider the changes of incremental stresses after a failure wave occurs in a plate impact problem. The incremental longitudinal and lateral stresses are given by

$$\Delta s_{11} = (\Delta s_d)_{11} - \Delta\sigma_m \tag{16a}$$

and

$$\Delta s_{22} = \Delta s_{33} = (\Delta s_d)_{22} - \Delta \sigma_m \tag{16b}$$

respectively. Because the macroscopic strain field is unchanged in the failure zone behind the elastic shock wave, it follows from Eqs. (5), (6) and (15) that

$$\begin{aligned} \Delta s_{11} &= -2G\left(\Delta e_d^i\right)_{11} - \frac{\partial \sigma_m}{\partial V_d}\Delta V_d \\ &= -\frac{4G\sigma_m (s_{11} - s_{22})}{3(V_0 + V_d)s_d : s_d}\Delta V_d - \frac{a_1 + 2a_2\mu_e + 3a_3\mu_e^2}{V}\Delta V_d \end{aligned} \tag{17a}$$

and

$$\begin{aligned} \Delta s_{22} &= \Delta s_{33} = -2G\left(\Delta e_d^i\right)_{22} - \frac{\partial \sigma_m}{\partial V_d}\Delta V_d \\ &= \frac{2G\sigma_m (s_{11} - s_{22})}{3(V_0 + V_d)s_d : s_d}\Delta V_d - \frac{a_1 + 2a_2\mu_e + 3a_3\mu_e^2}{V}\Delta V_d < 0 \end{aligned} \tag{17b}$$

As can be seen from Eq. (17), a zero change in the longitudinal stress might result in an increase in the absolute value of lateral stresses for a suitable value of V_d (Note that $s_{11} < s_{22} = s_{33} < 0$ in a plate impact problem). The effects of model parameters on the failure response will be demonstrated in Section 4.

The above damage model describes only the evolution of damage with time at a given material point. The interactions among different material points in a continuum, which result in the evolution of damage in space, must be modeled through an appropriate manner. Higher order models, such as nonlocal integral or strain gradient models, have been used to predict the evolution of localized failure, as reviewed by Chen and Schreyer (1994). However, the use of higher order models yields higher order governing differential equations, in addition to the ambiguity of additional boundary conditions. Another approach is to apply the jump conditions to different material domains so that the classical governing differential equations are still valid to simulate the evolution of localization (Chen and Sulsky, 1995; Chen and Xin, 1999). In this report, a three-dimensional damage diffusion equation that is based on the physical mechanisms of failure waves is formulated, as elucidated next, to predict the evolution of damage in space through the value of V_d. Since both the wave equation and diffusion equation are still the 2nd order partial differential equations, an effective numerical procedure can be developed with parallel computing for large-scale model-based simulation.

As indicated by Feng (2000), severe loading conditions at the impact surface, including the effect of impact tilt, may play the same role as the impact surface imperfection in initiating the failure wave in shocked glasses. If the plane of entering wave front is not exactly coincident with that of the material surface as it is usually the case in practice, the transient loading conditions on the surface involve a line of stress concentration sweeping across the surface. Because of the geometry, the confinement associated with this moving stress concentration is lower than that of the uniaxial strain and the loading rate can be significantly higher than that at the wave front inside the material. The combination of the severe loading conditions and inevitable surface imperfection may initiate isolated microcracking in the vicinity of the impact surface. Please note that the microscopic defects, if any, randomly distributed inside the specimen material should not be severe enough to initiate the failure wave, but will certainly speed up the failure evolution process inside the material. For the purpose of simplicity, however, the bulk of the material is assumed to be flawless so that the effect of randomly distributed microscopic defects is not considered here. Based on the above analysis, it appears to be reasonable to consider the impact surface as the only source for initiating the failure wave in shocked glasses. The formation of microcracks on the impact surface will in turn introduces local stress concentrations to the adjacent downstream material. Once these stress concentrations reach a certain threshold, microfissuring will be initiated there, and so on. Since the limitation of current computational capabilities does not allow a detailed modeling of the evolution of each individual microcrack, the failure propagation process can be described by a progressive percolation of microfissures in an average sense. Based on the physics involved, this process is macroscopically of diffusive nature, i.e., a diffusion process starting from a high concentration of microcracks to a low concentration of microcracks until a saturated state is reached in the continuum or discontinuous failure occurs. To activate the diffusion process, both microscopic heterogeneity and sufficient deviatoric strain energy are required as long as it is initiated. If either the heterogeneity or deviatoric strain energy is not large enough, the diffusion process will not be active or die out eventually. From a viewpoint of energy conservation, the evolution of a failure wave in space converts the deviatoric strain energy in the intact material ahead of the failure front into the volumetric potential energy in the comminuted

material behind the front. As a result, there is a decrease in the stress deviator and an increase in the mean stress in the uniaxial strain condition.

It should be pointed out that even if the shock wave compression is along the longitudinal direction, the percolation of microfissures occurs three-dimensionally. Therefore, a three-dimensional diffusion equation must be formulated to govern the percolation of microfissures, which is measured in terms of the dilated volume, as discussed before. In a standard form, the diffusion equation in the three-dimensional space $\boldsymbol{x}$ with time t can be written as

$$\frac{\partial V_d}{\partial t} = \nabla \bullet [\boldsymbol{D}(\boldsymbol{x},t) \bullet \nabla V_d] \tag{18}$$

where $\boldsymbol{D}(\boldsymbol{x},t)$ denotes the second order damage diffusivity tensor. Although the rate of percolation in the lateral direction is different in general from that in the longitudinal direction, the existing experimental data do not warrant the detailed formulation of $\boldsymbol{D}(\boldsymbol{x},t)$. If the microscopic details of percolation in different orientations are not pursued, it is reasonable to let $\boldsymbol{D}(\boldsymbol{x},t) = D(\boldsymbol{x},t)\boldsymbol{i}$ with

$$D(\boldsymbol{x},t) = \begin{cases} 0 & \text{if } Y \le Y_{THD} \text{ or } V_d = 0 \\ d\dfrac{Y - Y_F}{Y_{HEL} - Y_F} \ge 0 & \text{if } Y > Y_{THD} \text{ or } V_d > 0 \end{cases} \tag{19}$$

where d is the isotropic diffusion coefficient, and $Y = \sqrt{\frac{3}{2}\boldsymbol{s}_d : \boldsymbol{s}_d}$ (In a plate impact problem, $Y = |s_{11} - s_{22}|$). The parameters Y_{HEL} and Y_F represent the stress deviators in the intact material at the HEL and in the damaged material at the completion of failure process, respectively. As can be seen from Eq. (19), the diffusion is inactive if the stress deviator is below the threshold Y_{THD}, or if the dilated volume is equal to zero. As long as $Y > Y_{THD}$ or $V_d > 0$, the diffusion process will start until $Y = Y_F$. Unloading occurs when $Y < Y_F$. Since certain time is required for the lateral microdamage percolation to finish at a given longitudinal location, introduce a time-dependent evolution function into Eq. (18), which is defined by

$$Q(\boldsymbol{x},t) = \frac{D(\boldsymbol{x},t)}{d}\frac{V_d - V_{d0}}{T_d} \ge 0 \tag{20}$$

with V_{d0} being the threshold below which $Q(x,t)$ is inactive, and T_d denoting the characteristic time of the damage evolution at the longitudinal location. As a result, Eq. (18) then becomes

$$\frac{\partial V_d}{\partial t} = \nabla \bullet [D(x,t)\nabla V_d] + Q(x,t) \tag{21}$$

The effect of lateral percolation on the longitudinal percolation is reflected through the addition of $Q(x,t)$.

As can be seen from the above description, the proposed constitutive model includes the equations governing the strain-stress response at the local level, which mainly consists of Eqs. (2-4, 6, 15), and the equations governing the damage diffusion, namely, Eqs. (19-21).

The propagation of a failure wave is simulated through the evolution in both temporal and spatial domains of the internal state variable, V_d. If a specimen is shocked beyond the threshold Y_{THD} and an initial value of $V_d\,(>V_{d0})$ is assigned to the vicinity of the impact surface, a failure wave will propagate, behind the leading elastic shock wave, through the specimen that is assumed to be originally flawless ($V_d = 0$). Although V_d increases during the damage diffusion, the specific volume of the compressed material, V, remains constant, and so do the macroscopic longitudinal stress and particle velocity. The increase of V_d results in the decrease of the deviatoric potential energy, as reflected through the increase of lateral stresses. In other words, the deviatoric potential energy in the intact material is converted into the volumetric potential energy in the comminuted and dilated material during the time-dependent failure evolution process.

It is expected that the material parameters for describing the damage diffusion, namely, d, Y_{THD}, Y_F, V_{d0} and T_d, can be evaluated via well-defined impact experiments that measure the damage evolution profile and the residual frictional strength of comminuted material. To solve both the usual equation governing the shock wave propagation and the proposed damage diffusion equation in a single computational domain, a simple numerical procedure is described in the next section.

3. Numerical Procedure

The numerical procedures for conventional wave and diffusion equations can be found in the standard books (Belytschko and Hughes, 1983; Reddy and Gartling, 1994; among others). In this report, central-difference in space and forward integration in time are used to solve the diffusion equation, while constant stress elements in space and an explicit time integrator are employed to solve the wave equation.

To implement the differential form of the proposed damage model into the shock wave code, the updated Lagrangian formulation is used so that the matrix equations of displacement-based finite elements can be written as

$$[M]\{\ddot{u}\}^t = \{R\}^t - \{F\}_t^t + \{P\}_t^t \tag{22}$$

where $[M]$ is the time-independent diagonal mass matrix, $\{\ddot{u}\}^t$ the vector of nodal accelerations at time t, $\{R\}^t$ the vector of externally applied nodal loads at t, $\{F\}_t^t$ the vector of internal nodal forces at t measured with respect to the configuration at t, and $\{P\}_t^t$ the vector of viscous damping nodal forces at t measured with respect to the configuration at t. Thus, the velocity strain tensor can be obtained in each time step to find the corresponding Cauchy stress tensor through the constitutive model. Based on the Cauchy stresses, the internal nodal forces can then be calculated with respect to the current configuration. To produce a sharp shock wave front, the viscous damping nodal forces are introduced into Eq. (22), which are obtained from element damping stresses. For each constant stress element e at time t, the damping stress takes the form of

$$q_e^t = \frac{\Delta\rho_e}{\Delta t^t}\left(v_l c_l \sqrt{A_e^t} + v_q \frac{\overline{A}_e |\Delta\rho_e|}{\overline{\rho}_e \Delta t^t} \right) i \tag{23}$$

if $\left|\rho_e^t - \rho_e^0\right| \geq 10^{-7}\, kg/m^3$. In Eq. (23), v_l and v_q are the linear and quadratic coefficients of artificial viscous stress, with $v_l = 0.95$ and $v_q = 1.0$ being chosen for numerical demonstration in the next section. c_l is the current longitudinal wave speed. The incremental mass density, the average mass density and the average area are defined by

$$\begin{cases} \Delta\rho_e = \rho_e^t - \rho_e^{t-\Delta t'} \\ \overline{\rho}_e = \frac{1}{2}\left(\rho_e^t + \rho_e^{t-\Delta t'} \right) \\ \overline{A}_e = \frac{1}{2}\left(A_e^t + A_e^{t-\Delta t'} \right) \end{cases} \tag{24}$$

The time step is estimated as follows:

$$\Delta t^{t+\Delta t'} = min\left[0.9\Delta t_l,\ max\left(1.2\Delta t^t,\ 0.035\Delta t_l\right)\right] \tag{25.1}$$

with

$$\Delta t_l = \Delta t\left(1 - 3v_t\right)\left(\sqrt{v_l^2 + 1} - v_l\right) \tag{25.2}$$

in which Δt is the estimated time step without including the artificial viscosity in Eq. (22), and $v_t = 0.1$ is chosen here.

Although the wave and diffusion equations are coupled in terms of V_d after failure occurs, a simple procedure is adopted here to solve the wave and diffusion equations in a parallel (staggered) setting, with the time step satisfying both stability conditions in a single computational domain.

4. Demonstration and Verification

To demonstrate and verify the proposed model and solution procedure, the shock experiments chosen by Feng (2000) will be considered here, which reveal most clearly the quantitative nature of the failure wave phenomenon, as compared with other existing data.

It should be pointed out that there is no complete set of data in the open literature which could be used to verify the model parameters, although the failure wave phenomenon has been observed in several kinds of shocked glasses. In the recent experimental characterization of the failure response of mortar under impact loading (Grote et al., 2000), no data are available to evaluate Eqs. (3) and (4) because the elastic properties are assumed to be constant in the shock response. Hence, the experimental data, which have been collected from several sources in a way as consistent as possible (Feng, 2000), are used here to verify the proposed model.

Based on the wave profile measurements and mean stress response for a soda lime glass, the original mass density, longitudinal and shear sound speeds, and apparent HEL stress of the material are given by $\rho_0 = 2530kg/m^3$, $c_L = 5828m/s$, $c_s = 3468m/s$ and $\sigma_{HEL} = 5.95GPa$, respectively. It follows from a Lagrangian analysis that Eqs. (3) and (4) become

$$\sigma_m = 45.36\mu_e - 137.00\mu_e^2 + 288.30\mu_e^3 \tag{26}$$

and

$$G = 30.43\mu_e + 1.49\sigma_m - 0.60\sigma_m^2 - 0.35\sigma_m^3 \tag{27}$$

where the units of σ_m and G are *GPa*. The stress deviators at the HEL and the threshold for initiating the failure wave are $Y_{HEL} = 4.53GPa$ and $Y_{THD} = 2.24GPa$ (which corresponds to a shock stress of *3 GPa*), respectively. The longitudinal and lateral gauge data on a shocked K-8 glass (Kanel et al., 1991) are used to compare with the model prediction. Since the shock stress in the experiment was close to the specimen material's HEL of about *8 GPa*, which is significantly higher than that of the model material ($\sigma_{HEL} = 5.95GPa$), a normalization procedure is used here to minimize the effects of inherent material property differences. It is assumed that the failure process would result in a 50% increase in the lateral stress, at which $Y = Y_F$ so that $D(x,t) = 0$ in Eq. (19), in accordance with the experimental data. Both the experimental and numerical results are then normalized with respect to their respective lateral stresses ahead of the failure front. The original time correlation between the data profiles at different locations is unknown. For clarity, a time correlation based on a sound speed of *5828m/s* is incorporated in the data. The model parameters related to damage diffusion, which match the data, are found to be $d = 12m^2/s$, $T_d = 7.7\times10^{-9}s$ and $V_{d0} = 2.0\times10^{-7}m^3/kg$. As shown in Fig. 1, the model predicts the essential feature of the experimental data. The longitudinal stresses corresponding to the lateral stresses are shown in Fig. 2. As can be seen, there is almost no change in the longitudinal stress during the failure evolution. It should be pointed out that Feng (2000) used an ad hoc approach in 1-D modeling and simulation so that the longitudinal stress must be fixed to find the corresponding lateral stress. Without fixing the longitudinal stress, however, the 3-D damage model proposed here can predict the essential features of the observed failure wave phenomenon. The effects of model

parameters, which control the diffusion process, are illustrated in Figs. 3 and 4. The profiles of V_d and corresponding effective stresses with time are shown in Figs. 5 and 6, which are consistent with the model formulation. Due to the effect of lateral percolation, the effective stress is decreasing with the increase of V_d during the failure propagation.

To simulate the transition from continuous to discontinuous failure modes in the future work, the Material Point Method (MPM), which was recently developed for those problems such as penetration, perforation, metal forming and cutting (Sulsky et al., 1994), has been employed here to solve the failure wave problem. Figures 7-12 demonstrate the numerical solutions obtained via the MPM, corresponding to Figs. 1-6. As can be seen, both the FEM and MPM yield the same solution features for the same problem, although the spatial discretization procedure used in the FEM is different from that in the MPM. It appears that the numerical dispersion of the MPM is more obvious than the FEM, a further discussion on which is beyond the scope of this report.

5. Concluding Remarks and Future Research

To provide a general framework for modeling the impact response of certain materials, a three-dimensional continuum damage model has been developed in this report, based on the assumption of shear-induced dilatancy. The essential component of the proposed model is that the deviatoric potential energy in the intact material is converted into the volumetric potential energy in the comminuted and dilated material during the time-dependent failure evolution process. The progressive percolation of microfissures is described by a nonlinear diffusion equation throughout the continuum body. The diffusion equation and wave equation are then solved via a staggered manner in a single computational domain. Numerical solutions, obtained via both the FEM and MPM, have been presented and verified with experimental data available. It appears that the essential features of the failure wave phenomenon, as observed in shock experiments on glasses, can be predicted by the proposed approach.

Although a considerable progress has been made in understanding the failure wave phenomenon since it was reported about 10 years ago, well-defined experiments are still needed to provide a consistent set of experimental data to verify the constitutive modeling and solution procedures. A combined experimental, analytical and

computational effort is a necessity for us to fully understand the physics involved in formation and propagation of failure in impact problems.

Acknowledgments

This work was sponsored (in part) by the Air Force Office of Scientific Research, USAF, under grant/contract number F49620-96-1-0381. The interests shown by Maj. Felice and Maj. Chipley are gratefully acknowledged. The author is also grateful to Prof. R. Feng at the University of Nebraska-Lincoln for valuable joint discussions on failure waves in shocked glasses, and to Mr. X. Xin for the computing assistance.

Referennces

Belytschko, T., Hughes, T., editors, 1983. *Computational Methods for Transient Analysis* **1**, Elsevier Science Publishers B.V.

Bless, S.J., Brar, N.S., 1994. Impact Induced Fracture of Glass Bars. *High-Pressure Science and Technology* (Edited by S.C. Schmidt, J.W. Shaner, G.A. Samana and M. Ross). AIP, New York, NY, pp. 1813-1816.

Bourne, N.K., Rosenberg, Z., Field, J.E., 1995. High-Speed Photography of Compressive Failure Waves in Glasses. *Journal of Applied Physics* **78**, 3736-3739.

Brar, N.S., Bless, S.J., Rosenberg, Z., 1991. Impact-Induced Failure Waves in Glass Bars and Plates. *Applied Physics Letter* **59**, 3396-3398.

Chen, Z., 1996. Continuous and Discontinuous Failure Modes. *Journal of Engineering Mechanics* **122**, 80-82.

Chen, Z., Clark, T., 1995. Some Remarks on Domain-Transition Problems. *Archives of Mechanics* **47**, 499-512.

Chen, Z., Schreyer, H.L., 1994. On Nonlocal Damage Models for Interface Problems. *International Journal of Solids and Structures* **31**, 1241-1261.

Chen, Z., Sulsky, D., 1995. A Partitioned-Modeling Approach with Moving Jump Conditions for Localization. *International Journal of Solids and Structures* **32**, 1893-1905.

Chen, Z., Xin, X., 1999. An Analytical and Numerical Study of Failure Waves. *International Journal of Solids and Structures* **36**, 3977-3991.

Clifton, R.J., 1993. Analysis of Failure Waves in Glasses. *Applied Mechanics Reviews* **46**, 540-546.

Espinosa, H.D., Xu, Y., Brar, N.S., 1997a. Micromechanics of Failure Waves in Glass: Experiments. *Journal of the American Ceramic Society* **80**, 2061-2073.

Espinosa, H.D., Xu, Y., Brar, N.S., 1997b. Micromechanics of Failure Waves in Glass: Modeling. *Journal of the American Ceramic Society* **80**, 2074-2085.

Feng, R., 2000. Formation and Propagation of Failure in Shocked Glasses. Accepted for publication in *Journal of Applied Physics.*

Grady, D.E., 1995a. Dynamic Properties of Ceramic Materials. Technical Report SAND94-3266, Sandia National Laboratories, Albuquerque, NM.

Grady, D.E., 1995b. Shock Properties of High-Strength Ceramics. Technical Memorandum TMD G0395, Sandia National Laboratories, Albuquerque, NM.

Grote, D.L., Park, S.W., Zhou, M., 2000. Experimental Characterization of the Dynamic Failure Behavior of Mortar under Impact Loading. Submitted for publication in *Journal of Applied Physics.*

Kanel, G.I., Rasorenov, S.V., Fortov, V.E., 1991. The Failure Waves and Spallations in Homogeneous Brittle Materials, In: Schmidt, S.C., Dick, R.D., Forbes, J.W., Tasker, D.G. (Eds.), Shock Compression of Condensed Matter. Elsevier, New York, pp. 451-454.

Raiser, G., Clifton, R.J., 1994. Failure Waves in Uniaxial Compression of an Aluminosilicate Glass. *High-Pressure Science and Technology* (Edited by S.C. Schmidt, J.W. Shaner, G.A. Samana and M. Ross), pp. 1039-1042. AIP, New York, NY.

Raiser, G.F., Wise, J.L., Clifton, R.J., Grady, D.E., Cox, D.E., 1994. Plate Impact Response of Ceramics and Glasses. *Journal of Applied Physics* **75**, 3862-3869.

Reddy, J.N., Gartling, D.K., 1994. *The Finite Element Method in Heat Transfer and Fluid Dynamics*. CRC Press.

Rosenberg, Z., Bourne, N.K., Millett, J.C.F., 1996. Direct Measurements of Strain in Shock-Loaded Glass Specimens. *Journal of Applied Physics* **79**, 3971-3974.

Sulsky, D., Chen, Z., and Schreyer, H.L. (1994). A Particle Method for History-Dependent Materials. *Computer Methods in Applied Mechanics and Engineering* **118**, 179-196.

Tzou, D.Y., 1989. On the Thermal Shock Wave Induced by a Moving Heat Source. *ASME Journal of Heat Transfer* **111**, 232-238.

Tzou, D.Y., 1997. *Macro- to Microscale Heat Transfer: The Lagging Behavior.* Taylor & Francis, Washington, DC.

Xin, X., Chen, Z., 2000. An Analytical Solution with Local Models for the Evolution of Dynamic Softening. *International Journal of Solids and Structures* **37**, 5855-5872.

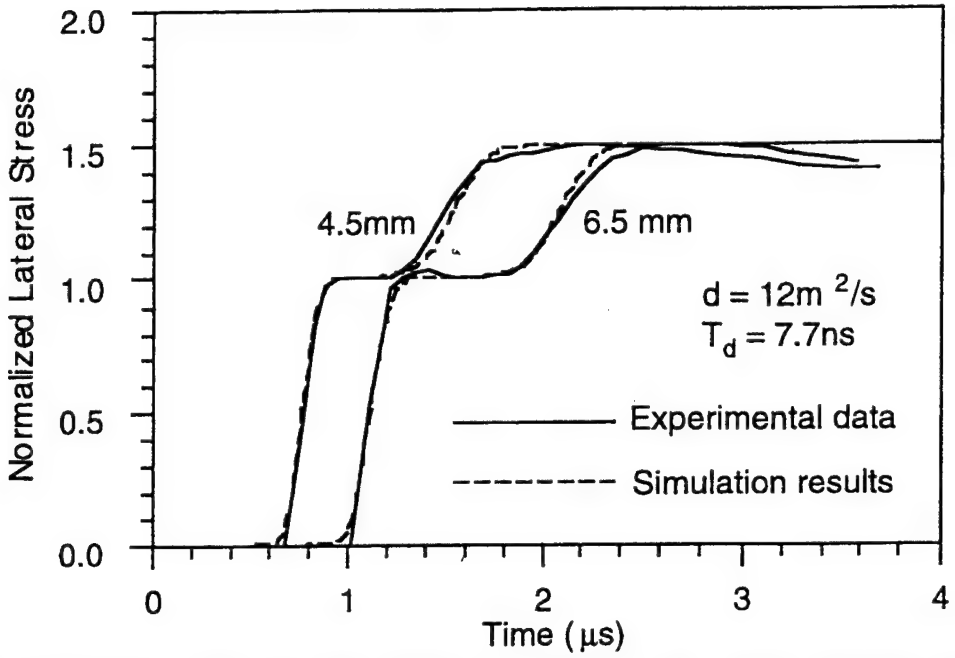

Figure 1. Comparison of the model prediction with experimental data.

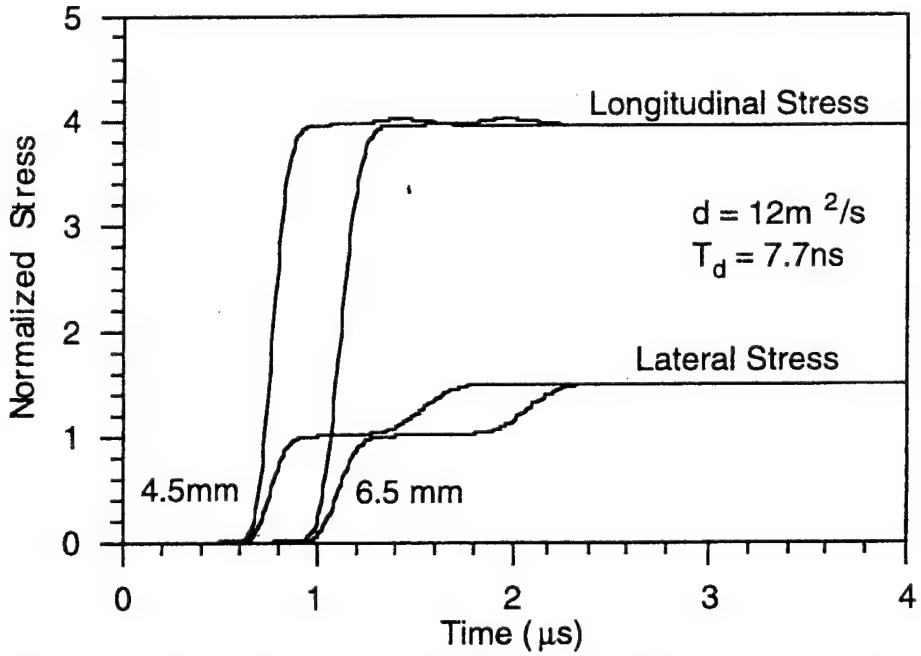

Figure 2. The longitudinal and lateral stresses of model prediction corresponding to Fig. 1.

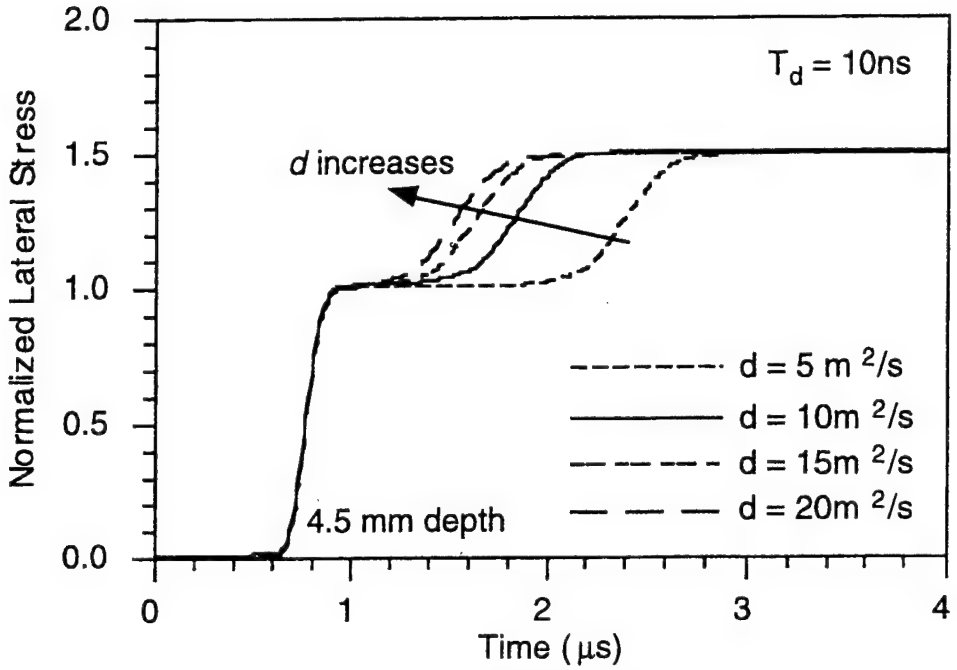

Figure 3. Effect of damage diffusivity.

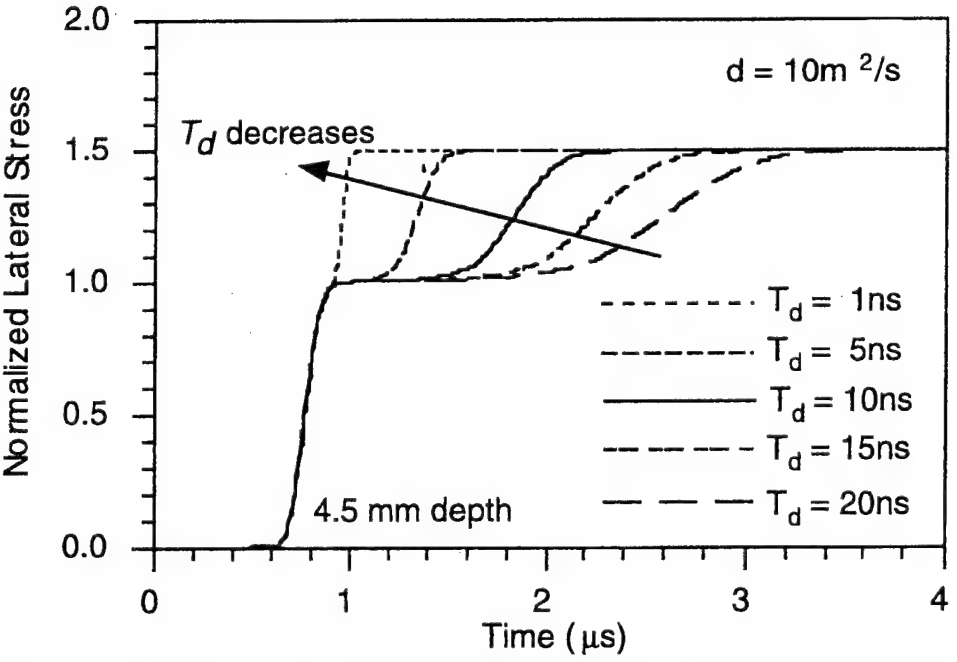

Figure 4. Effect of the characteristic time of damage evolution.

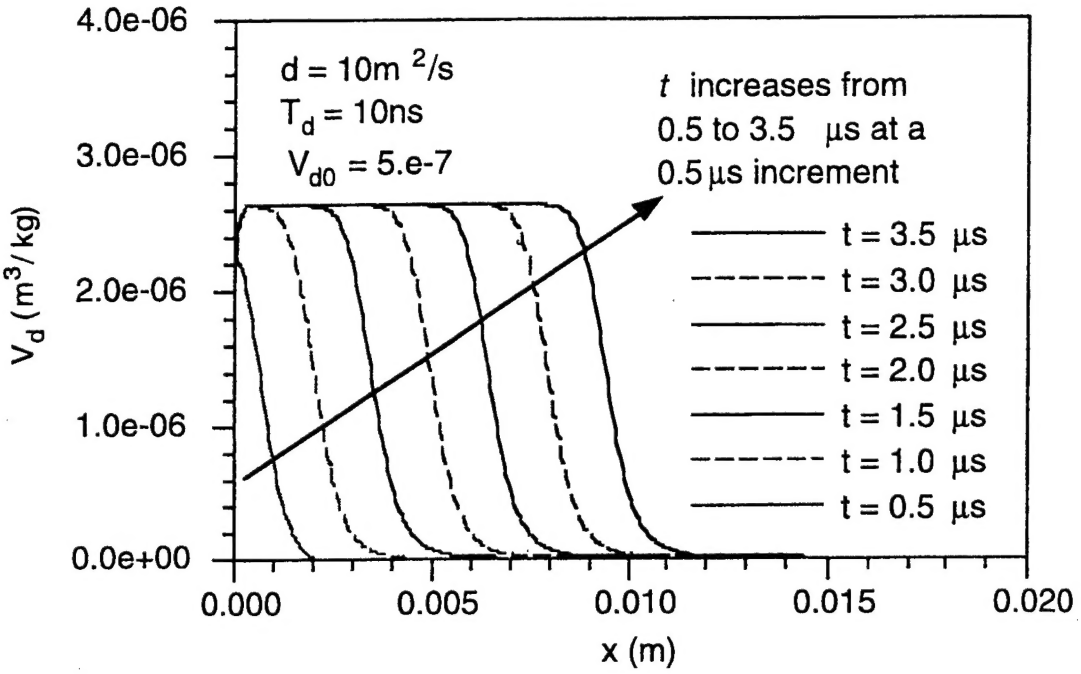

Figure 5. The profiles of Vd at different times.

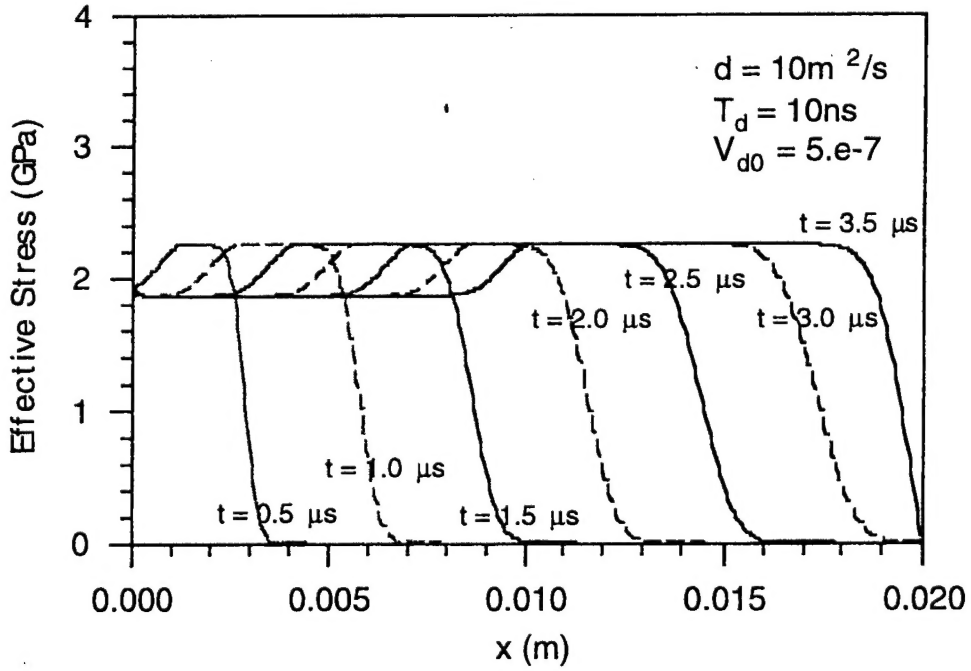

Figure 6. The profiles of effective stresses corresponding to Fig. 5.

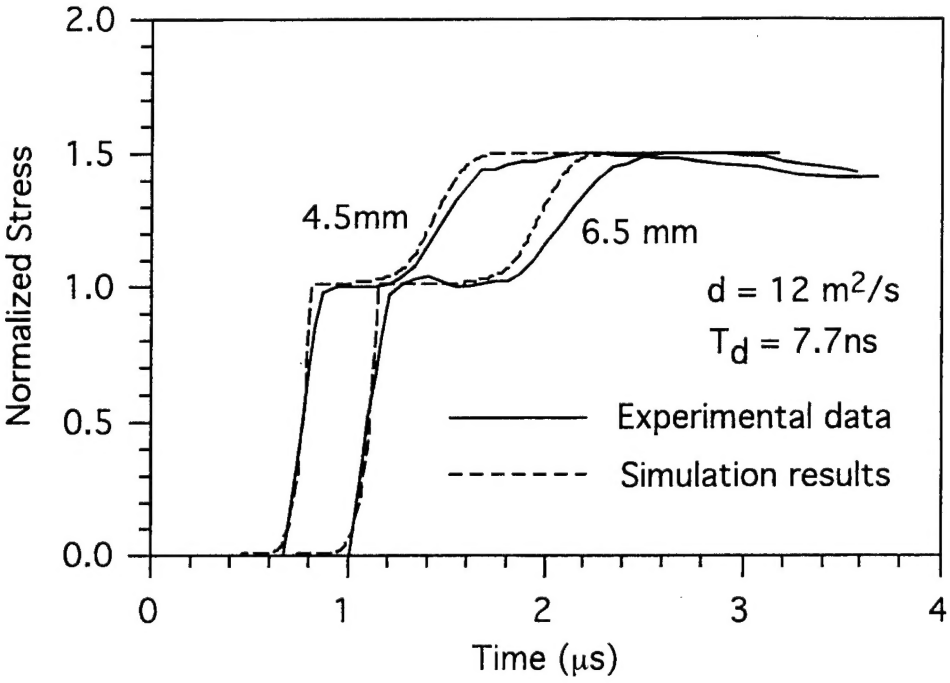

Figure 7. Comparison of the model prediction with experimental data, by using MPM.

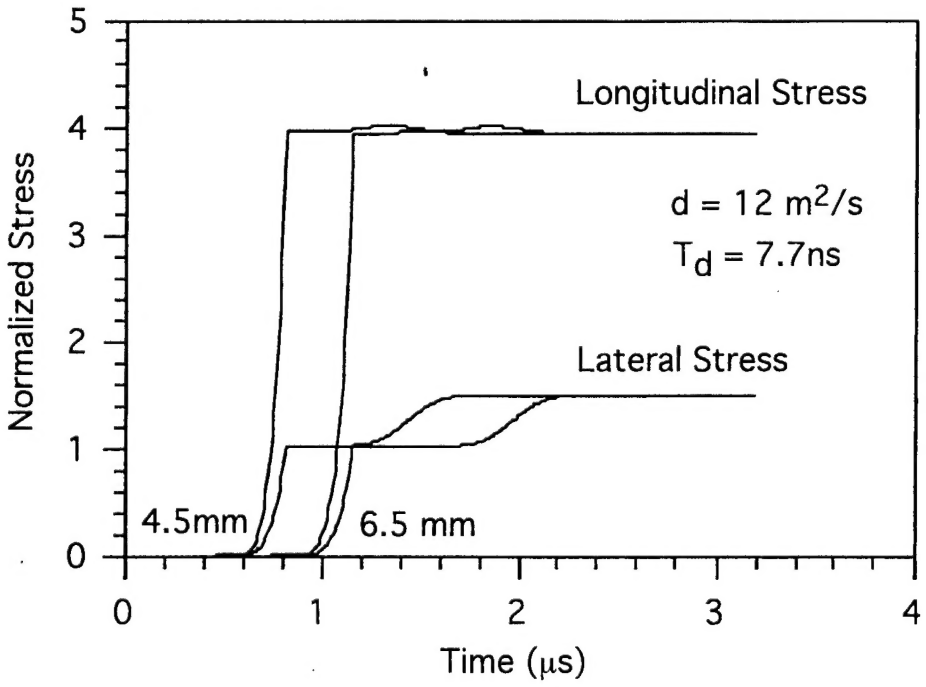

Figure 8. The longitudinal and lateral stresses of model prediction corresponding to Fig. 7, by using MPM.

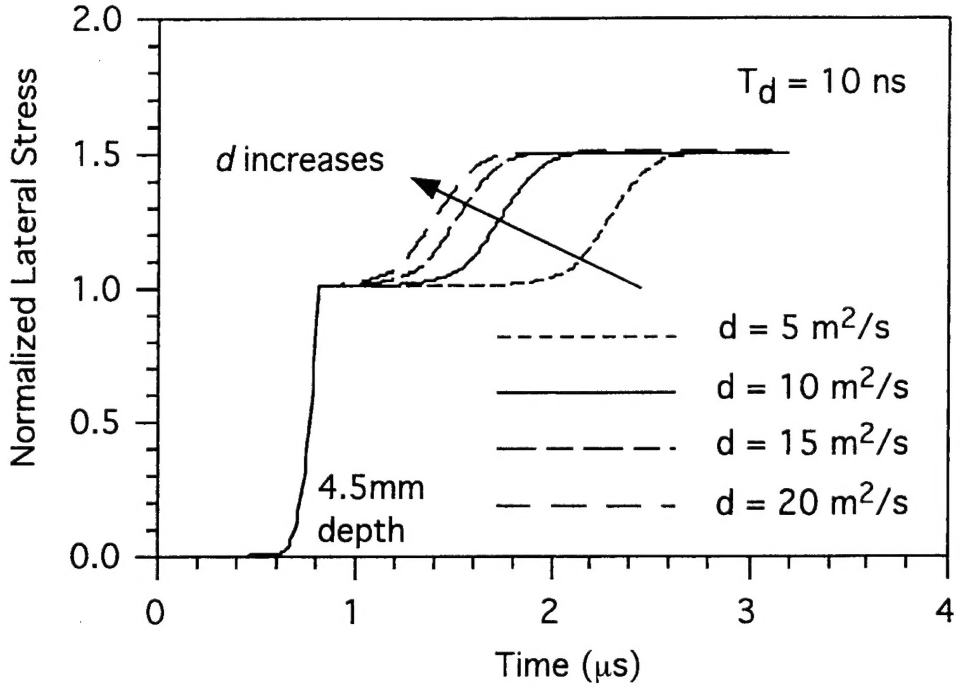

Figure 9. Effect of damage diffusivity, by using MPM.

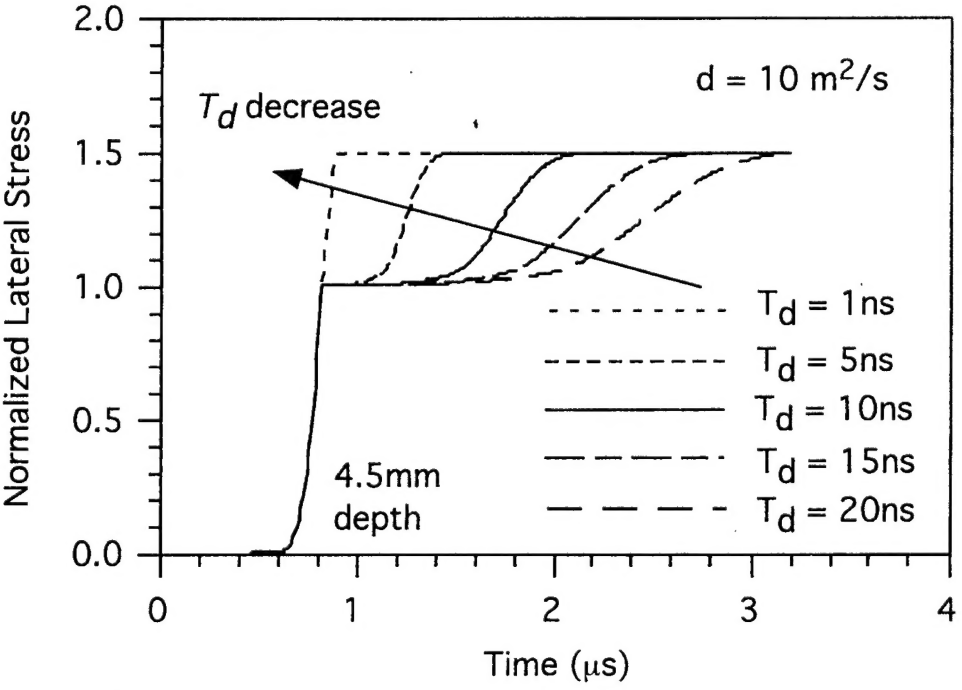

Figure 10. Effect of the characteristic time of damage evolution, by using MPM.

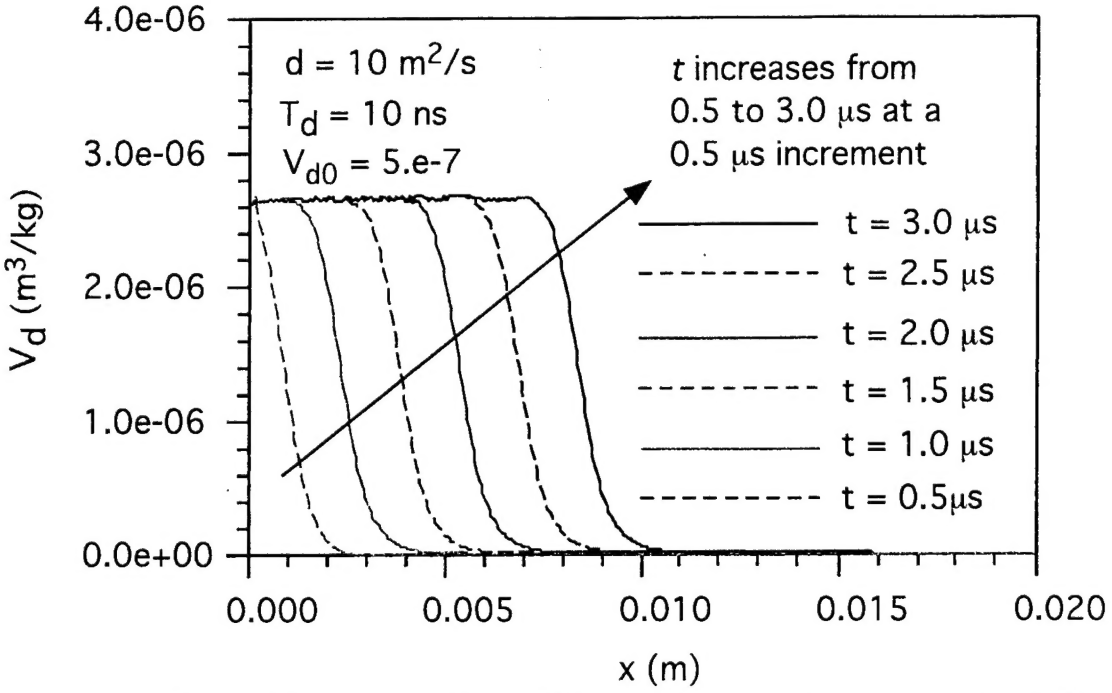

Figure 11. The profiles of V_d at different times, by using MPM.

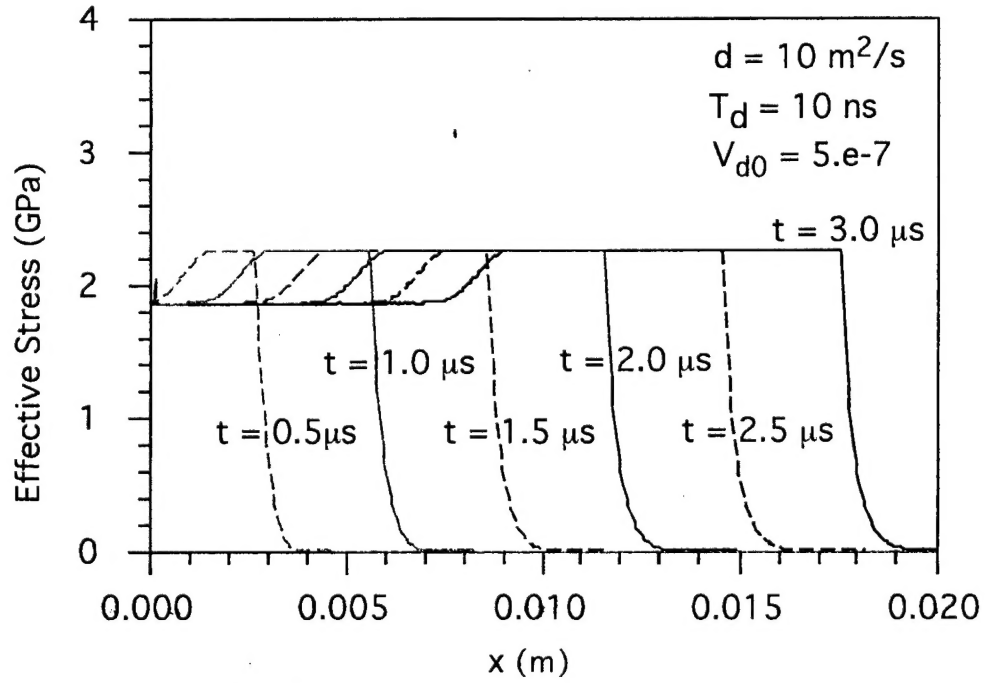

Figure 12. The profiles of effective stresses corresponding to Fig. 11, by using MPM.